



HAL
open science

Synergistic effect between hydrophobic oxide nanoparticles and ammonium polyphosphate on fire properties of poly(methyl methacrylate) and polystyrene

N. Cinausero, N. Azema, José-Marie Lopez-Cuesta, M. Cochez, M. Ferriol

► To cite this version:

N. Cinausero, N. Azema, José-Marie Lopez-Cuesta, M. Cochez, M. Ferriol. Synergistic effect between hydrophobic oxide nanoparticles and ammonium polyphosphate on fire properties of poly(methyl methacrylate) and polystyrene. *Polymer Degradation and Stability*, 2011, 96 (8), pp.1445-1454. 10.1016/j.polymdegradstab.2011.05.008 . hal-00772219

HAL Id: hal-00772219

<https://hal.science/hal-00772219>

Submitted on 27 Jul 2023

HAL is a multi-disciplinary open access archive for the deposit and dissemination of scientific research documents, whether they are published or not. The documents may come from teaching and research institutions in France or abroad, or from public or private research centers.

L'archive ouverte pluridisciplinaire **HAL**, est destinée au dépôt et à la diffusion de documents scientifiques de niveau recherche, publiés ou non, émanant des établissements d'enseignement et de recherche français ou étrangers, des laboratoires publics ou privés.

Synergistic effect between hydrophobic oxide nanoparticles and ammonium polyphosphate on fire properties of poly(methyl methacrylate) and polystyrene

N. Cinausero^a, N. Azema^a, J.-M. Lopez-Cuesta^a, M. Cochez^b, M. Ferriol^{b,*}

^a Centre des Matériaux de Grande Diffusion, Ecole des Mines d'Alès, 6 avenue de Clavières, 30319 ALES Cedex, France

^b Laboratoire MOPS EA 4423, Département Chimie de l'IUT de Moselle Est, Université Paul Verlaine-Metz, 12 rue V. Demange, 57503 Saint-Avold Cedex, France

A B S T R A C T

Synergism on fire properties has been investigated between nano sized hydrophobic oxides (alumina and silica) and ammonium polyphosphate (AP) flame retardant additive. Thermal degradation of mixed additives (50% w/w) showed the impact of oxides on AP degradation. The effect of modified nano particles was compared with corresponding hydrophilic oxide as regards thermal and fire behaviour. The nanocomposites prepared by melt blending were evaluated by thermogravimetric analysis and cone calorimetry measurements. Residues were characterized by ATR FTIR spectroscopy, X ray diffraction and SEM EDX experiments. A noteworthy decrease of peak of heat release rate and smoke opacity as well as an increase of LOI were noticed with hydrophobic silica combined with AP both in PMMA and PS. This flame retardant behaviour was ascribed mainly to the formation of a specific silicon metaphosphate (SiP_2O_7) crystalline phase which contributes to promote charring and an efficient insulating layer.

Keywords:

Flame-retardancy
Thermal stability
Nanocomposites
Barrier effect
Surface treatment
Silica

1. Introduction

Many scientific works have shown the interest in the incorporation of various kinds of nanoparticles to improve thermal stability and fire retardancy of polymers [1–4]. Mechanisms of fire retardancy induced by mineral nanoparticles and particularly by organomodified layered silicates have been detailed by various authors [5–8], highlighting physical effects such as formation of mineral barriers able to limit volatile and oxygen transfer, formation of carbonaceous residues due to catalytic processes. Metal oxide nanoparticles have been investigated in various polymers, particularly in PMMA and their influence on thermal degradation of polymer has been ascribed to several processes [4,9–11]:

- restriction of polymer chain mobility,
- high thermal diffusivity of particles increasing the heat transfer inside the material,
- trapping effect of radicals emitted from the polymer during polymer degradation.

In the case of PMMA, antagonistic processes on thermal stability involving interactions between hydroxyl groups of oxide and methoxycarbonyl groups of PMMA can occur, depending on the temperature and nano oxide loading [12,13].

In order to avoid adverse catalytic effects on the thermal degradation of polymers, surface treatments of metallic nano oxides can be considered. Moreover, it can be expected that these treatments could enhance some functional properties of nano composites, by the following mechanisms:

- promotion of the nanoparticles dispersion or migration in the molten state,
- improvement of the cohesion between grafted nanoparticles and polymer chains by interdiffusion,
- enhancement of the thermal stability and fire retardancy due to surface treatments including active compounds on flame retardancy like phosphorus compounds.

This last mechanism can be illustrated by a study [14] in which we performed both grafting and polymerization of ethylene glycol methacrylate phosphate on alumina nanoparticles using the “grafting through” method. As a result, a decrease of the peak heat release rate (HRR) was observed for PMMA and PS nanocomposites containing such modified particles.

Previously, we investigated also the interest to combine hydrophilic nanometric alumina and titanium dioxide particles with phosphorus flame retardants (ammonium polyphosphate and aluminum phosphinate) in order to improve the fire retardancy of PMMA [15,16]. Synergistic effects on HRR values and thermal stability between the nano oxides and ammonium polyphosphate (AP) or phosphinate were only noticed for alumina. The

efficiency of alumina stems from the formation of a compact carbonaceous structure reinforced by crystalline structures $Al_2P_6O_{18}$, resulting from interactions between Al_2O_3 and a decomposition product of AP (P_4O_{10}). This protective layer seems able to limit mass transfers of both methyl methacrylate and oxygen. Regarding the differences between the influence of aluminum and titanium dioxide on the morphology of the surface layer formed, it was observed that the crystalline structure built from titanium dioxide (TiP_2O_7 and $Ti(PO_4)_4$) and AP conferred only a porous and heterogeneous character, leading to a poor fire behaviour.

Concerning synergistic effects on fire behaviour of phosphorus and aluminum compounds in polystyrene, Cui et al. [17] have noticed such effects between red phosphorus and aluminum trihydroxide (ATH) in HIPS. The residual structure formed after combustion exhibited a better cohesion than ones with red phosphorus or ATH alone in HIPS.

The objective of this paper is precisely to investigate if AP/nano oxide combinations could be effective in a polymer such as PS presenting a different degradation pathway than PMMA. Moreover, this work aims to investigate the influence of hydrophobic/hydrophilic character of two kinds of oxide nanoparticles (silica and alumina) on possible synergistic effects on flame retardancy occurring with nano oxide/AP combinations.

Hence, various combinations of pristine (hydrophilic) or octylsilane treated (hydrophobic) alumina and silica with AP and PMMA or PS have been prepared at a total loading of 15 wt%. Evaluations of flame retardancy of these compositions were made using both cone calorimeter and limiting oxygen index test. A particular attention has been focused on the composition and microstructure of residues in order to interpret the differences observed concerning flame retardancy.

2. Experimental

2.1. Materials

Pellets of PMMA (Altuglas V 825T, Arkema) and PS (Total Petrochemicals, crystal PS 1960N) were size reduced in powder in a Pallman crushing machine before blending with additives.

Commercial hydrophilic alumina, designated in the following by "Alu" (Aeroxide Alu C, Evonik Degussa), and hydrophobic alumina modified with octylsilane, designated by "Alu C8" (Aeroxide Alu C 805, Evonik Degussa), were both 13 nm average diameter nanoparticles. Likewise, hydrophilic silica "Sil" and hydrophobic silica "Sil C8" supplied by Evonik Degussa (respectively Aerosil 200 and Aerosil R805) have both average diameters of 12 nm. Ammonium polyphosphate (AP) was donated by Clariant (Exolit AP 423).

Table 1
Compositions of PMMA and PS nanocomposites.

Compositions	PMMA	PS	AP	Alu	Alu-C8	Sil	Sil-C8
PMMA	100						
PMMA/AP 15%	85		15				
PMMA/AP 10%/Alu 5%	85		10	5			
PMMA/AP 10%/Alu-C8 5%	85		10		5		
PMMA/AP 10%/Sil 5%	85		10			5	
PMMA/AP 10%/Sil-C8 5%	85		10				5
PS		100					
PS/AP 15%		85	15				
PS/AP 10%/Alu 5%		85	10	5			
PS/AP 10%/Alu-C8 5%		85	10		5		
PS/AP 10%/Sil 5%		85	10			5	
PS/AP 10%/Sil-C8 5%		85	10				5

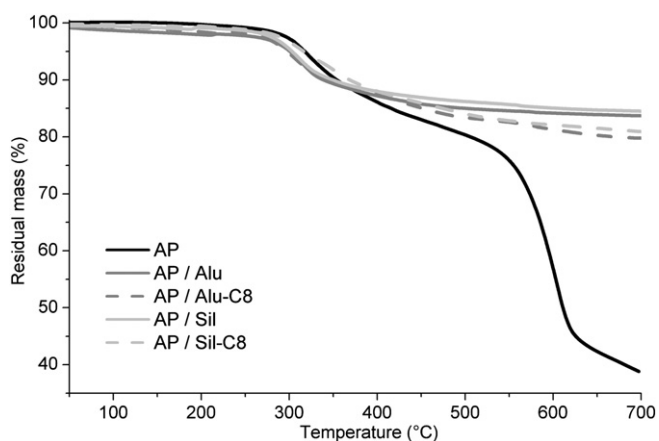


Fig. 1. TGA curves (50–700 °C) of pure ammonium polyphosphate and mixed with nanofillers (50% w/w).

2.2. Instrumentation

Thermogravimetric analyses (TGA) were performed with a Perkin Elmer Pyris 1 TGA thermobalance operating in air and with alumina crucibles containing around 10 ± 2 mg of material. The runs were carried out under dynamic conditions at the heating rate of $10^\circ\text{C}/\text{min}$ from room temperature to 700°C .

Flammability tests were performed with the limiting oxygen index (LOI) test, according to the ISO 4589 standard, using a Stanton Redcroft instrument on barrels ($80\text{ mm} \times 10\text{ mm} \times 4\text{ mm}$).

Evaluation of fire reaction of polymers and nanocomposites was made using a cone calorimeter device (Fire Testing Technology). Sheets ($100\text{ mm} \times 100\text{ mm} \times 4\text{ mm}$) were exposed to a radiant cone under a heat flux of $35\text{ kW}/\text{m}^2$. Time to ignition (TTI), time of flammability (TOF), total heat release (THR), peak of heat released rate (pHRR), Mass Loss Rate (MLR) and amount of residue after burning will be discussed. Results correspond to mean values obtained from two or three experiments. Residues of samples after cone calorimeter test were collected and crushed finely to be observed with X ray diffraction, EDX and ATR FTIR.

X ray diffraction patterns were recorded at room temperature on a BRUKER D8 X ray powder diffractometer fitted with a fast analyzer and using $\text{Cu } K_\alpha$ radiation.

The C/Si and C/Al ratios in the carbonaceous residues were determined by Energy Dispersive X ray analysis (EDX) linked with a scanning electron microscope FEI Quanta 200.

Finally, ATR FTIR spectra were recorded at room temperature on a Bruker IFS66 FTIR spectrometer (Golden Gate reflection system) to analyse the carbonaceous residues of nanocomposites. The spectra were measured with a spectral resolution of 2 cm^{-1} .

2.3. Preparation of nanocomposites

Samples were prepared by mixing polymer powder and flame retardant additives in a Haake PolyLab internal mixer at 225°C for

Table 2
Maximum degradation rate temperatures and amount of residues of AP/oxides mixtures.

Composition	T_{dm1} (°C)	T_{dm2} (°C)	T_{dm3} (°C)	Residue (%)
AP	322		603	38.8
AP/Alu	315			83.7
AP/Alu-C8	306			79.8
AP/Sil	311			84.5
AP/Sil-C8	315	353		80.9

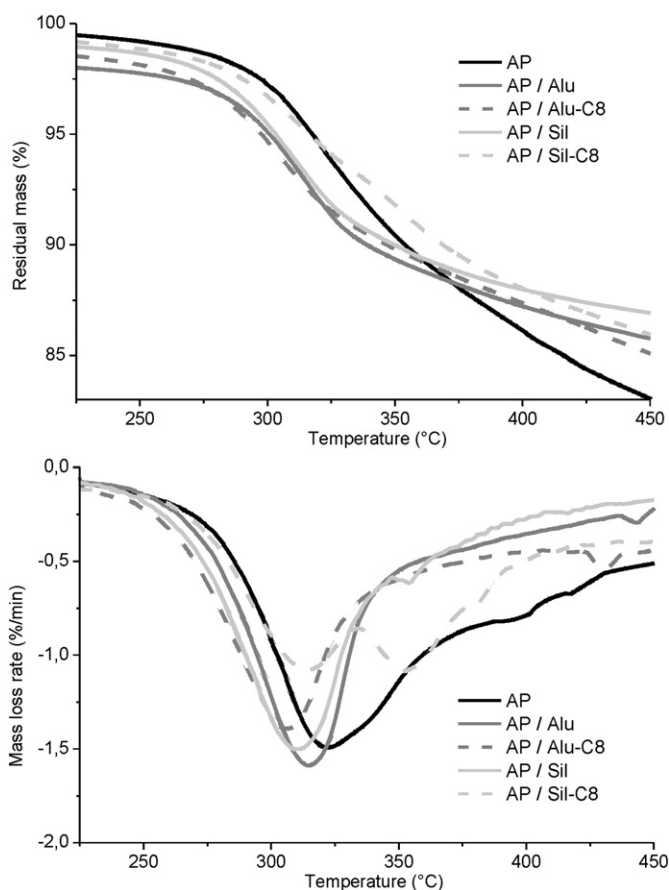


Fig. 2. TGA and DTG curves (225–450 °C) of pure ammonium polyphosphate and mixed with nanofillers.

PMMA (200 °C for PS) and 50 rpm. Flame retarded compositions were based on 15 wt% of ammonium polyphosphate (AP) in polymer whereas binary systems were made from a substitution of 5 wt% of AP by nano oxides (Table 1). The total mixing time was typically 8 min. The resulting nanocomposites were crushed in Alpine rotary cutter mill before being compression moulded at

225 °C for 5 min at 100 bar to obtain the sheets used for cone calorimeter measurements. The same procedure was applied to pristine polymers in order to compare properly with filled compositions.

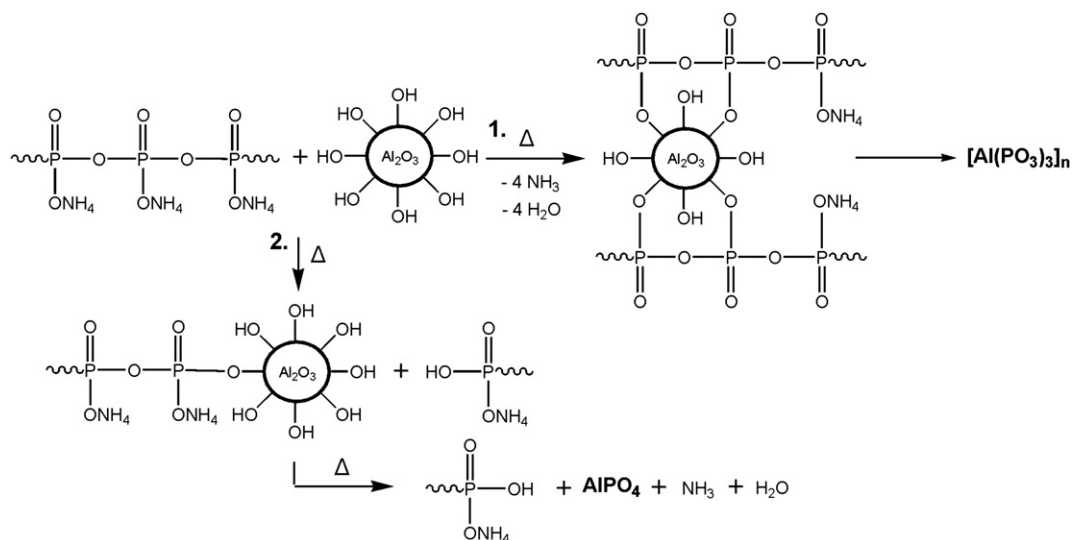
3. Results and discussion

3.1. Thermal analyses of additives

So as to highlight possible interactions between flame retardant additives, AP/oxides mixed powders (50% w/w) were analysed by TGA (Fig. 1). Thermal degradation of AP is well known as a two step mechanism [18,19]. First weight loss starts from 250 °C and corresponds to elimination of H₂O and NH₃ characterized by a maximal degradation peak centred at 322 °C. Release of water causes the formation of phosphoric acid, followed by crosslinking into vitreous ultraphosphate. Second decomposition step is the fragmentation of ultraphosphate to P₂O₅ and phosphate compounds at higher temperatures (Table 2).

Residual products representing less than 40% of initial AP are likely to be thermally stable P–N compounds. When oxides are mixed with AP, the first degradation step is shifted to lower temperatures respectively of 7 °C and 11 °C for hydrophilic oxides. An enlargement of 225–450 °C temperature range shows clearly (Fig. 2) that AP loses much less volatiles than AP/oxides mixture.

Indeed at 250 °C for instance, AP loses 0,8 wt% of its weight when it is heated alone and 4.5 wt% in presence of alumina (weight loss of AP/Alu mixture in TGA is 2.25% at 250 °C). Silica has a weaker effect on water and ammonia releases than alumina. Furthermore, surface modification of these oxides tends to limit this catalytic effect of NH₃ and H₂O release below 270 °C, which could be induced by the reactivity of hydroxyl groups. Moreover, a stabilization effect is observed between 250 °C and 400 °C for AP/Sil C8 system, modifying the first main weight loss in two distinct peaks at 315 °C and 353 °C. In the temperature range 450–700 °C, the second weight loss of AP does not occur when AP and oxides are mixed together. Thus, decomposition of intermediate species such as polyphosphoric acid into P₂O₅ does not take place assuming strong interactions between oxides and phosphorus compounds. These types of interactions were exhibited by Castrovinci et al. [20] between ammonium polyphosphate and aluminum trihydroxide in SBR. An orthophosphate AlPO₄ and an aluminum metaphosphate



Scheme 1. Possible reactions occurring between AP and Al₂O₃.

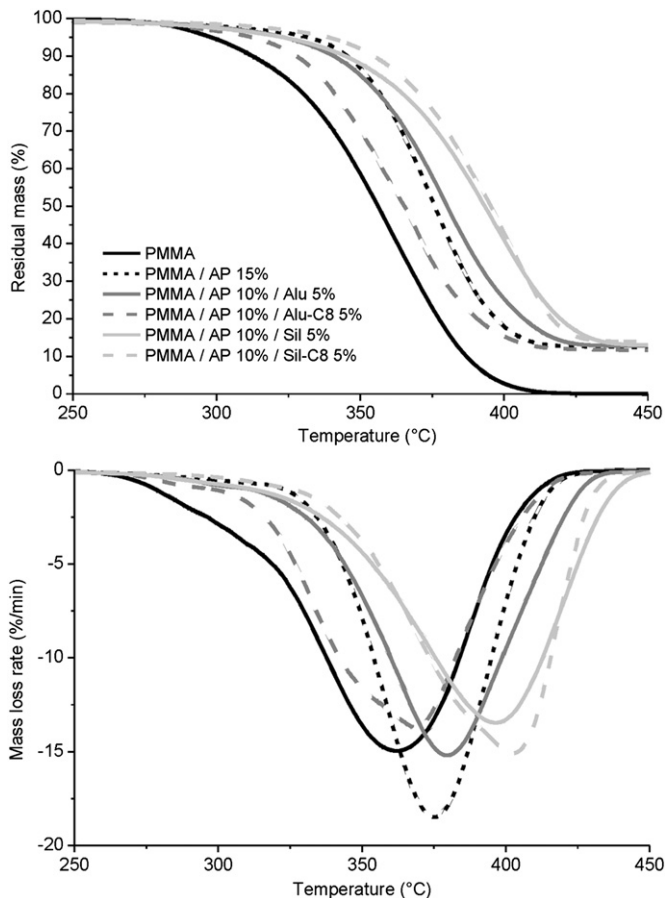


Fig. 3. TGA and DTG curves under air of PMMA nanocomposites.

phase $[\text{Al}(\text{PO}_3)_3]_n$ were created during heating. The authors observed that these crystalline structures did not bring enhancement of thermal stability by disrupting both efficient and continuous shield of ultraphosphate. Based on this previous study, Scheme 1 illustrates how Al_2O_3 and AP could interact between themselves releasing water and ammonia.

3.2. Thermo oxidative degradation of nanocomposites

3.2.1. PMMA nanocomposites

Fig. 3 displays thermo oxidative degradation of PMMA, PMMA/AP 15% and PMMA nanocomposite compositions. Addition of 15 wt % of ammonium polyphosphate increases initial degradation temperature ($T_{2\%}$) of 23 °C (Table 3). The phenomenon is ascribed to modifications of degradation pathway of PMMA [18]. Trans esterification reactions occur between decomposition products of

Table 3
2% degradation and maximum degradation rate temperatures of PMMA and PS nanocomposites.

Compositions	$T_{d2\%}$ (°C)	T_{dm} (°C)	Compositions	$T_{d2\%}$ (°C)	T_{dm} (°C)
PMMA	276	362	PS	322	405
PMMA/AP 15%	299	375	PS/AP 15%	322	408
PMMA/AP 10%/Alu 5%	296 (-3)	380 (+5)	PS/AP 10%/Alu 5%	316 (-6)	434 (+29)
PMMA/AP 10%/Alu-C8 5%	285 (-14)	369 (-6)	PS/AP 10%/Alu-C8 5%	327 (+5)	431 (+26)
PMMA/AP 10%/Sil 5%	292 (-7)	396 (+21)	PS/AP 10%/Sil 5%	335 (+13)	443 (+38)
PMMA/AP 10%/Sil-C8 5%	310 (+11)	403 (+28)	PS/AP 10%/Sil-C8 5%	332 (+10)	443 (+38)

AP, polyphosphoric acid, and polar groups of PMMA. Then, acid anhydrides result from cyclisation reactions, and their decomposition at higher temperatures leads to unsaturation along polymer backbone. These double bonds could stop depolymerisation of PMMA and promote char formation. Besides, AP might limit as well the disadvantageous catalytic effect of oxygen, as it is well known that PMMA is sensitive to thermo oxidation. Addition of hydrophilic alumina and silica lowers slightly initial degradation temperature which may be the result of higher amount of non combustible gases evolved from AP in presence of oxides (Fig. 2). Above 370 °C, thermal degradation of PMMA is slowed down likely due to barrier effect of crystalline structure induced by interactions between AP and oxide. Degradation rate reaches a peak at 403 °C for PMMA/AP 15%/Sil 5% composition, that is almost 30 °C higher than the reference PMMA/AP 15%. Systems combined with hydrophobic nanoparticles behave differently according to chemical composition of oxide. Indeed, hydrophobic silica Sil C8 brings an additional stabilization compared to Sil nanoparticles. Conversely, an antagonistic effect of Alu C8 favours the release of decomposition products up to 700 °C. As we concluded in another study [14], decomposition of octylsilane grafted on oxide may engender reactive radicals reliable to act on thermal degradation of PMMA. Thus, thermal behaviour of PMMA composites cannot be tackled only by physical explanations, but also by chemical considerations.

3.2.2. PS nanocomposites

Fig. 4 shows the TGA and DTG curves of PS, PS/AP 15%, and PS nanocomposites between 250 and 500 °C under air atmosphere. Unlike PMMA, decomposition of PS/AP 15% follows thermal

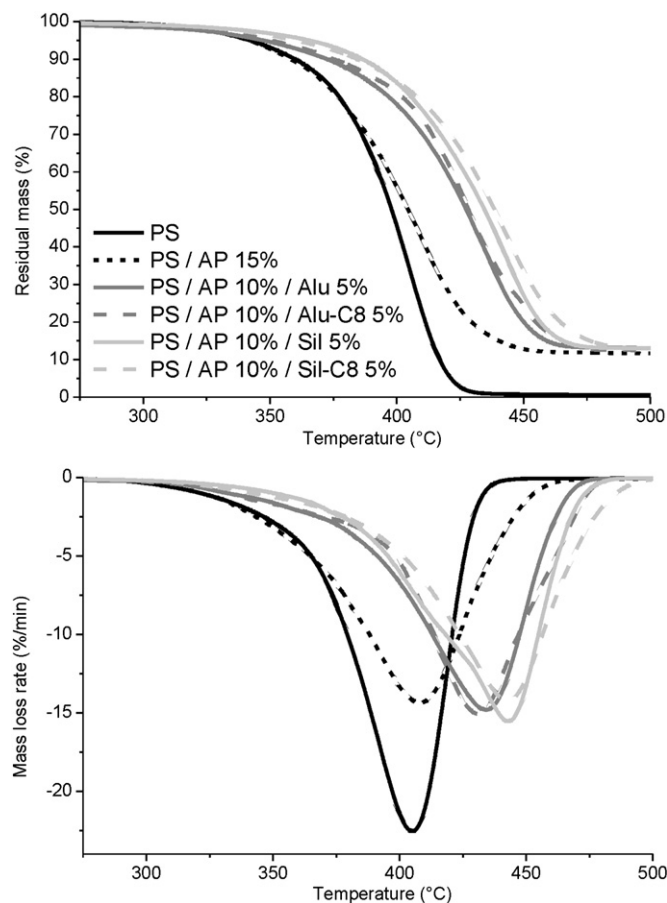


Fig. 4. TGA and DTG curves under air of PS nanocomposites.

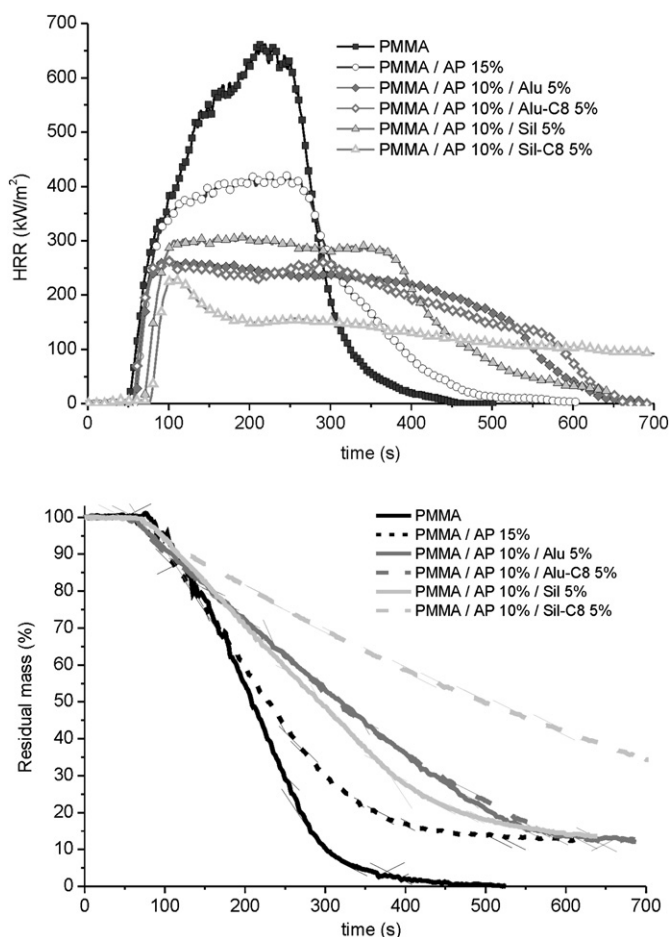


Fig. 5. HRR curves of PMMA and its nanocomposites.

Table 4

Cone calorimeter data of PMMA nanocomposites.

	TTI, s	TOF, s	THR, MJ/m ²	TSR, m ² /m ²	pHRR, kW/m ²	MLR, mg/s	Residue %	LOI
PMMA	57 ± 2	484 ± 33	126 ± 2	479 ± 44	639 ± 7	115 ± 8		18.0
PMMA/AP 15%	56 ± 0	516 ± 25	108 ± 0	647 ± 44	419 ± 3	84 ± 3	12.5 ± 0.3	20.0
PMMA/AP 10%/Alu 5%	58 ± 2	566 ± 8	111 ± 0	627 ± 86	266 ± 0	77 ± 1	13.2 ± 0.5	21.0
PMMA/AP 10%/Alu-C8 5%	56 ± 5	592 ± 4	109 ± 1	296 ± 26	262 ± 2	74 ± 0	12.3 ± 0.3	20.0
PMMA/AP 10%/Sil 5%	69 ± 2	552 ± 17	109 ± 1	533 ± 31	313 ± 4	78 ± 2	13.5 ± 0.1	21.5
PMMA/AP 10%/Sil-C8 5%	65 ± 2	943 ± 43	105 ± 1	352 ± 68	231 ± 2	44 ± 2	16.8 ± 1.2	25.0

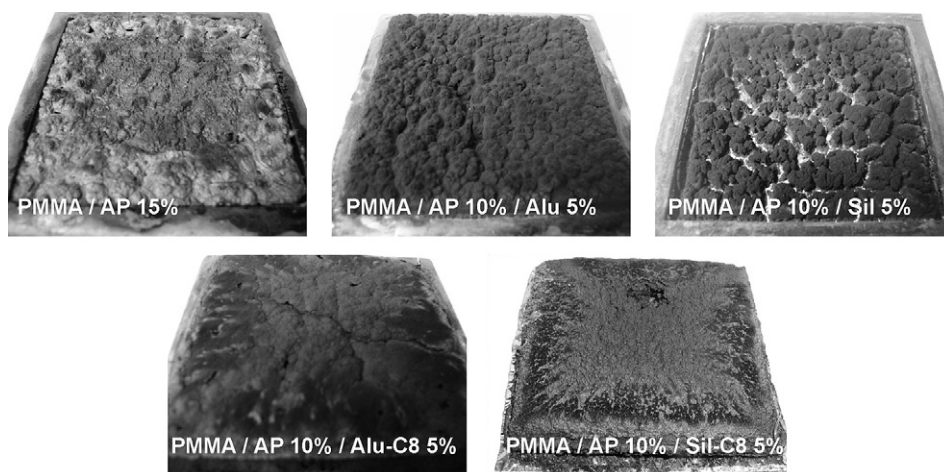


Fig. 6. Photographs of char residues after cone calorimeter experiments of PMMA samples.

behaviour of unfilled PS until 380 °C. Then, stabilization occurs and a char is formed. Czegeny et al. [21] explain that modifications of degradation pathway of PS occur in presence of ammonium polyphosphate and polyphosphoric acid. On the one hand, backbiting of PS is not favoured owing to a decrease of macroradical reactivity resulting from change of electron donating ability of the phenyl side group. On the other hand, interactions between ionic species of phosphorus additive and radical sites lead to cyclisation reactions and promote char formation. Replacement of flame retardant by 5% oxide increases thermal stability of nanocomposites by 30 °C and 40 °C as regards T_{dm} (Table 3). This increase comes not only from the stabilization effect of alumina and silica on PS thermal degradation (radical trapping, barrier effect, chain mobility), but also from a synergistic effect of the AP/oxide system. Finally, on the whole, surface modification does not bring any stronger thermal stability except during initial step of decomposition of Alu C8 based composition.

3.3. Fire reaction

3.3.1. PMMA nanocomposites

Fig. 5 and Table 4 present the results of cone calorimeter experiments of PMMA based compositions. During combustion of PMMA/AP 15%, small solid islands are formed and grow progressively but without ever covering entirely the surface. Release of gaseous degradation products of PMMA is strong and the final residue does not display any cohesion (Fig. 6), covering only edges of sample holder. After its withdrawal from heating cone after flameout, the residue becomes rapidly viscous due to the high amount of water trapped in ultraphosphate structure. Nevertheless, HRR peak and mass loss rate values decrease respectively of 34% and 27% compared to pure PMMA.

Substitution of AP by 5% oxide modifies notably fire reaction. Indeed, islands grow at sample surface from ignition and form a solid layer that avoids ebullition of decomposition products. Intumescent effect is observed only for alumina. Discontinuous

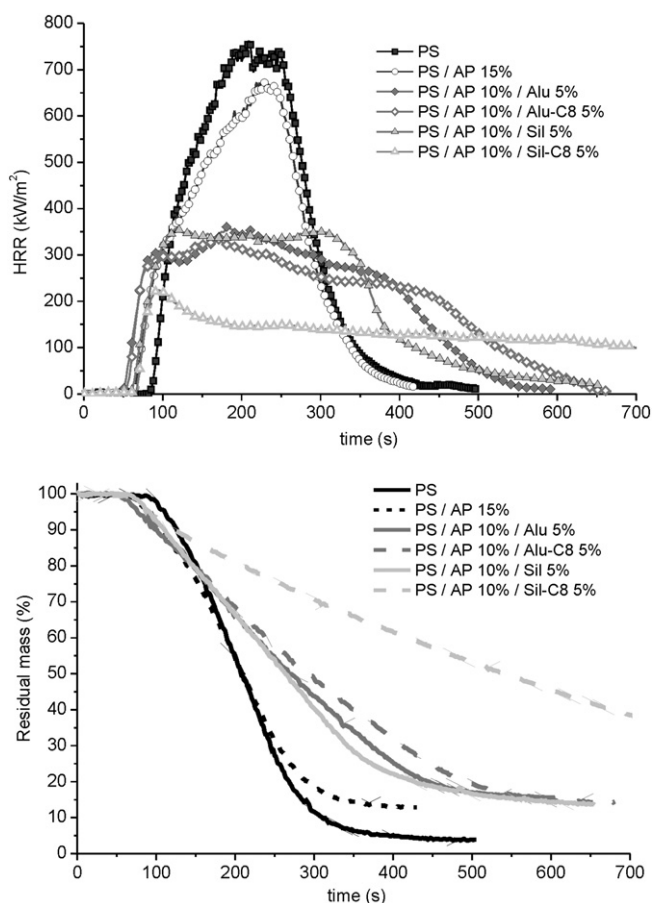


Fig. 7. HRR curves of PS and its nanocomposites.

char is observed with silica, whereas an efficient protection towards heat flux occurs with alumina. This behaviour can be one of the explanations of pHRR variation between both formulations (58% with Alu and 51% with Sil). Furthermore, two different macroscopic morphologies of char are noticed according to chemical nature of oxide. Aluminum based residues are “shell” structured: barrier protection is achieved at the surface of materials while material is consumed inside. It remains at the end of the test a hollow protective crust. At the contrary, charring effect of silica based residues is characterized by a “bulk” structure: shape of sample is maintained – despite cracks – and filled of carbonaceous matter.

Another cause of HRR decrease could be linked to different crystalline properties of char resulting from the AP/oxide interactions. Moreover, despite higher pHRR with PMMA/AP 10%/Sil 5%, silica has a positive effect on Time To Ignition (TTI) and smoke release. Decrease of THR is only related to the substitution of 15% of organic phase in composite. Finally, oxygen index is raised until

21.0 and 21.5 respectively with Alu and Sil instead of 20 for the phosphorus flame retardant used at 15 w%.

The use of modified alumina Alu C8 does not change the heat release rate compared to unmodified aluminum oxide, but decrease by more than 50% the total smoke release. Hydrophobic silica containing composition displays very interesting fire behaviour with peak of heat release rate lowered to 64% against the PMMA. Ignition of materials causes almost instantaneously the formation of a fine grey layer ($t = 100$ s) that becomes black straight after and covers then the entire sample surface ($t = 150$ s). Intumescent phenomenon occurs limiting considerably flame height and combustion level until end of test. Mass loss rate is decreased to 44 mg/s (84 mg/s for PMMA/AP 15%). Indeed at $t = 550$ s, only 50% of initial mass of sample is consumed when using Sil C8 while at such an exposure time final residues are almost formed for all others compositions, as displays Fig. 5. LOI is in accordance with this efficient flame retardant behaviour since it reaches 25.0. Smoke opacity is weak in spite of the long combustion of organic compounds taking place during 15 min (9 min for PMMA/AP 15%/Sil 5%).

3.3.2. PS nanocomposites

HRR and mass loss curves as well as cone calorimeter data are presented in Fig. 7 and Table 5. Despite charring effect of AP, the phosphorus additive does not bring improvement of fire behaviour: time to ignition is reduced and pHRR is comparable to the pristine PS. Inorganic residue is built under the molten polymer during combustion, which explains the absence of flame retardant efficiency. Besides, ignition arises 20 s before PS owing to release of combustible compounds catalysed by the presence of AP. That confirms modification of degradation pathway of PS induced by ammonium polyphosphate additives. Addition of hydrophilic nano oxides like alumina and silica leads to the formation of a solid protective layer and hence fire reaction is improved by a synergistic effect. pHRR values of both unmodified oxides containing compositions are comparable, even if a longer time is required to reach pHRR with alumina. Increase of HRR of PS/AP 10%/Sil 5% composition coincides with the apparition of numerous cracks at around $t = 250$ s. Besides, combustion of PS/AP 10%/Alu 5% composition undergoes an intumescent phenomenon but a discontinuous char surface is also observed (Fig. 8). Alumina has a catalytic effect on release of combustible products before ignition of PS since TTI decreases from 62 to 50 s whereas TTI is not altered in presence of silica compared to PS/AP 15% composition. Like PMMA nanocomposites, PS residues adopt different morphologies according to the use of alumina (shell structured) or silica (bulk structured).

Let us discuss now the influence of surface modified oxides. Hydrophobization of alumina tends to decrease HRR values from about $t = 170$ s (40 kW/m^2) as well as slightly the peak of heat release rate compared to hydrophilic alumina. This slowing down of combustion is clearly seen on mass loss curves (Fig. 7). These differences can be explained partly owing to a char more stable and less cracked using Alu C8 (Fig. 8). Synergy on fire properties

Table 5
Cone calorimeter data of PS nanocomposites.

	TTI, s	TOF, s	THR, MJ/m ²	TSR, m ² /m ²	pHRR, kW/m ²	MLR, mg/s	Residue %	LOI
PS	83 ± 0	401 ± 15	131 ± 0	5163 ± 1	752 ± 10	99 ± 4		18.5
PS/AP 15%	62 ± 9	375 ± 3	118 ± 1	4138 ± 74	690 ± 18	101 ± 0	13.3 ± 0.4	20.5
PS/AP 10%/Alu 5%	50 ± 1	590 ± 37	119 ± 2	4166 ± 233	342 ± 19	64 ± 4	14.8 ± 0.8	20.5
PS/AP 10%/Alu-C8 5%	53 ± 1	587 ± 37	119 ± 3	4259 ± 134	329 ± 7	66 ± 1	13.6 ± 0.9	20.0
PS/AP 10%/Sil 5%	61 ± 1	612 ± 30	118 ± 5	4358 ± 210	360 ± 3	62 ± 3	13.7 ± 0.0	19.5
PS/AP 10%/Sil-C8 5%	66 ± 7	1109 ± 4	119 ± 2	2760 ± 74	233 ± 9	32 ± 0	17.5 ± 0.1	23.0

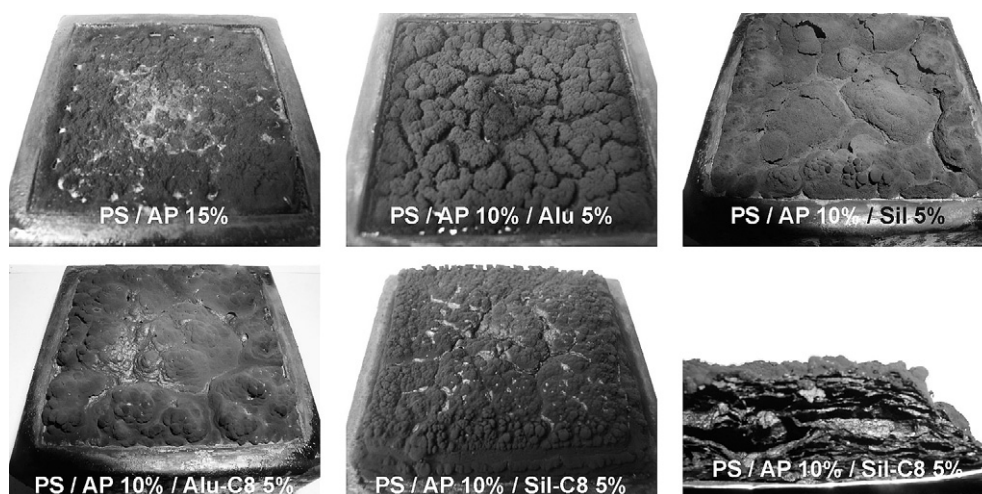


Fig. 8. Photographs of char residues after cone calorimeter experiments of PS samples.

between AP and Sil C8 in PMMA occurs also in PS. Thus, we can assume that these reactions which brought into play in the case of PMMA are not specific to this polymer matrix. Interactions between ammonium polyphosphate and octylsilane modified silica seem to be the main causes of fire behaviour enhancement. Thus, many parameters are improved as well in PS: time to ignition increases whereas pHRR is lowered to 70%, mass loss rates is twice lower than the other oxide containing compositions and smoke production is almost twice weaker than pristine PS one. Carbonaceous residue represents 17.5 wt% with Sil C8 against 13.7 wt% with hydrophilic silica. Let us focus now our attention on char pictures. Cross section of residue reveals a dense swelled char which is structured in layer. These different layers must contribute to limit gas and mass transfers as well as external heat flux. Finally, while all compositions have an oxygen index varying around 20.0, PS/AP 10%/Sil C8 5% has a LOI as high as 23.0 (18.5 for unfilled PS).

3.4. Analyses of residues

3.4.1. Analyses of residues by XRD

X ray diffraction spectra of oxide containing residues are displayed respectively Figs. 9 and 10. Concerning residues based

on alumina, diffraction pattern reveals the existence of a crystal line phase of aluminum metaphosphate which is liable to be either aluminum polyphosphates $[Al(PO_3)_3]_n$, or polymorphous cyclic phases of aluminum metaphosphate $Al(PO_3)_3$ [20,22]. Eventually, according to literature, the main phase in our Alu based residues seems to be type B aluminum metaphosphate, where PO_4 tetrahedra are linked together to form infinite (PO_3^-) chains [23]. These linear polyphosphates $[Al(PO_3)_3]_n$ would be formed from 300 °C. While surface treatment of alumina has no impact on crystalline phase with PS, Alu C8 engenders in PMMA the formation of crystalline phase $AlPO_4$ rather than aluminum polyphosphate. These trivalent cation monophosphates have atomic arrangements similar to the silica structure [22]. The formation of $AlPO_4$ results from chain scission reactions that imply more alumina than in the case of $Al(PO_3)_3$ phase. Thus, we can assume that AP/Alu C8 interactions are stronger than AP/Alu ones in PMMA. These observations highlight the possible link between crystalline structure and smoke release in PMMA since it was seen that Alu C8 divided the total smoke release by two.

In the case of siliceous residues, amorphous phase of nano metric silica detected by XRD is represented by a hump between $22^\circ < 2\theta < 28^\circ$. Besides, two different crystalline phases are present

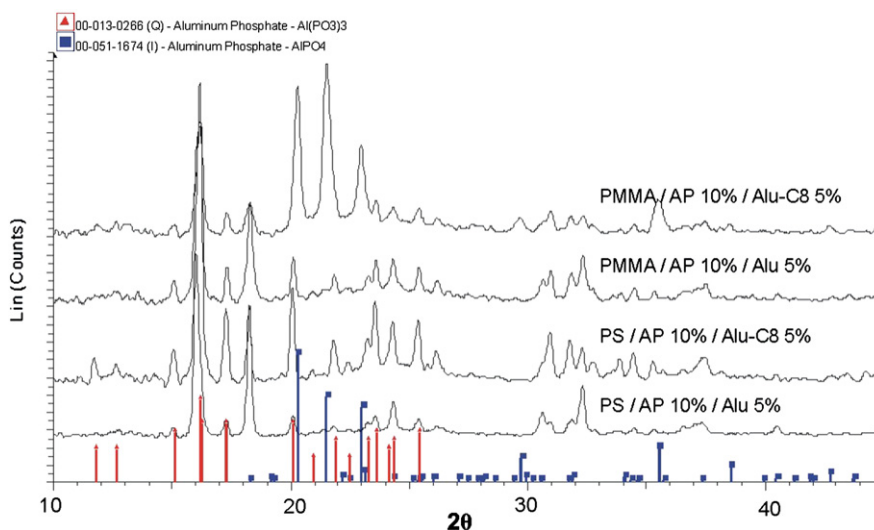


Fig. 9. X-ray diffraction spectra of alumina containing residues after cone calorimeter experiments.

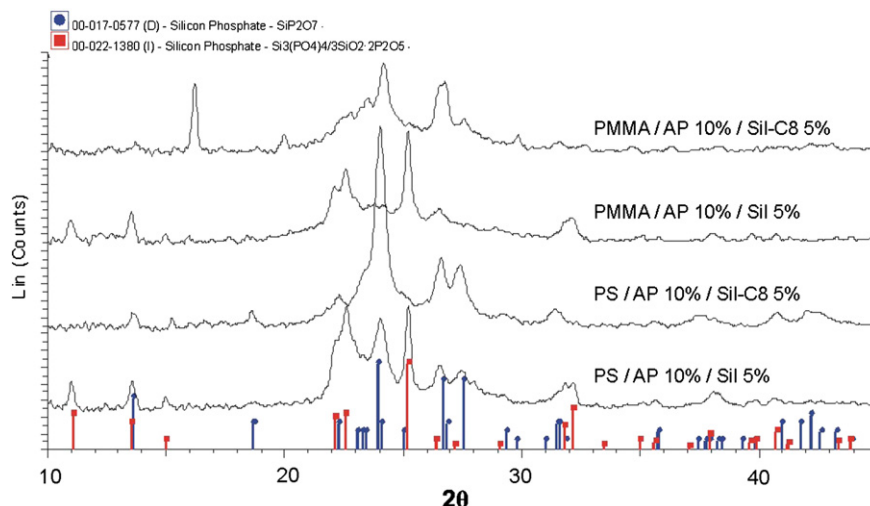


Fig. 10. X-ray diffraction spectra of residues after cone calorimeter experiments of silica containing residues.

on spectra and common to both polymers. The main phase is $\text{Si}_3(\text{PO}_4)_4$ whereas SiP_2O_7 crystals is represented as the minor phase formed during combustion. The presence of the latter is less clear in PMMA than in PS. Hydrophobic treatment of silica modifies the nature of crystals generated during cone calorimeter measurements. Indeed, only SiP_2O_7 becomes the main and unique phase detected by XRD. This silicon pyrophosphate (monoclinic phase), results typically from arrangements of tetrahedrons PO_4 and octahedrons SiO_6 with hexacoordinated Si atoms, being bonded to six different phosphate groups [24]. Thus, the modification surface of silica led to specific arrangement with ammonium polyphosphate during sample burning at cone calorimeter. The silicon pyrophosphate SiP_2O_7 may be related to the formation of highly efficient thermal barrier towards radiative heat source. Thus, it is assumed also that these specific arrangements of SiP_2O_7 may be initiated by the interactions of decomposition products of octylsilane modified silica and ammonium polyphosphate at relatively low temperatures (300–400 °C) as we demonstrated by TGA. Nevertheless, the presence of such a crystalline phase in PS/AP 10%/Sil 5% suggests that this crystalline phase cannot explain by itself the advantageous fire behaviour observed in AP/Sil C8 systems. To sum up, a crucial phenomenon has to occur during decomposition of Sil C8 and AP which would favour the formation of SiP_2O_7 crystalline phase rather than $\text{Si}_3(\text{PO}_4)_4$.

3.4.2. X ray microanalysis of residues

Elemental ratios C/Al and C/Si were measured so as to compare the level of carbonaceous matter in final residues (Fig. 11). These ratios were given in relation to Si and Al assuming that oxides

nanoparticles remained in condensed phase during combustion process. First of all, PS residues have a larger tendency to promote char formation than PMMA residues. But, the noteworthy influence concerns the influence of surface modification of oxides, above all with octylsilane modified silica. Alu C8 nanoparticles contribute to increase C/Al ratio only for PS while no effect is noted for PMMA based residues. Such results are in accordance with cone calorimetry since impact of Alu C8 on HRR was noticed only in PS nanocomposites. Likewise, Sil C8 nanoparticles increase C/Si ratio both in PMMA and PS compared to hydrophilic silica containing residues. Thus, modification of interphase tends not only to enhance barrier effect but also to promote char formation as well as reticulation reactions.

Besides, FTIR analyses were carried out on residues whose infrared spectra are displayed Figs. 12–14. Absorption bands of pristine ammonium polyphosphate, well described in literature [19,25], are compared with residues of compositions with 15 wt% of AP (Fig. 12). For pure AP, NH_4^+ groups absorb on various frequency ranges corresponding to symmetric stretching mode (3300–2600 cm^{-1}) and deformation mode (1430–1420 cm^{-1}) (Table 6). Stretching $\text{P}=\text{O}$ bonds frequencies are centred at 1242 cm^{-1} whereas $\text{P}-\text{O}-\text{P}$ inorganic backbone vibrates according to symmetric (1010 cm^{-1}) and antisymmetric (880 cm^{-1}) stretching modes [26]. IR spectra of PMMA/AP 15% and PS/AP 15% residues are similar. Intense peak centred at 870 cm^{-1} is ascribed to $\text{P}-\text{O}-\text{P}$ bonds of ultraphosphate while peaks at 980–970 cm^{-1} are relative to $\text{P}-\text{O}(-\text{Ar})$. $\text{P}=\text{O}$ bonds are still present in the residue as well as nitrogenous groups vibrating around 1420 cm^{-1} . Indeed, during decomposition of AP, NH_4^+ groups are not all eliminated. However,

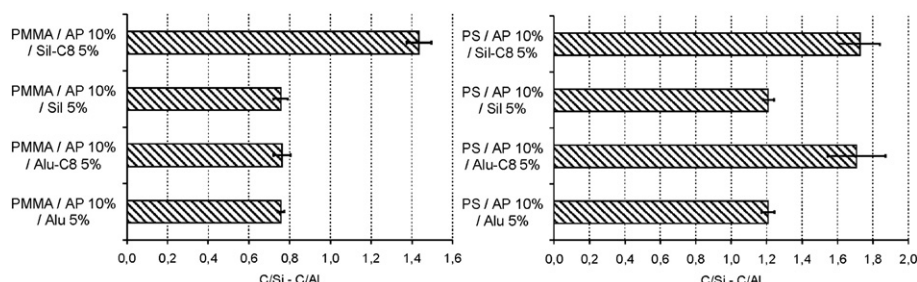


Fig. 11. Semi-quantitative X-ray microanalysis C/Al and C/Si of residues from cone calorimeter experiments.

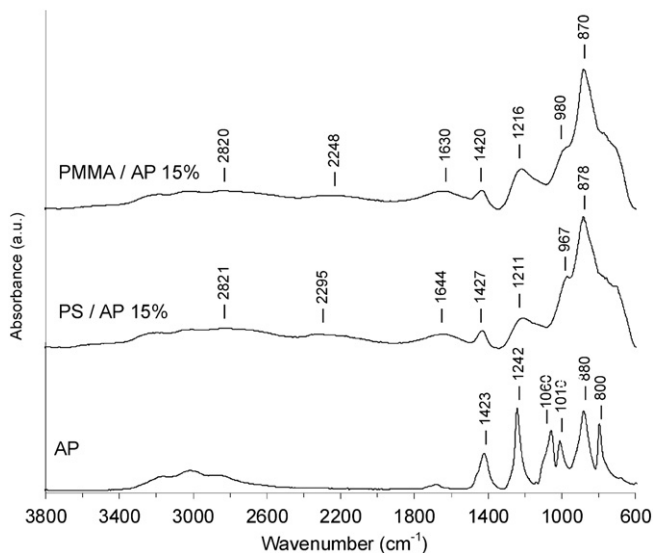


Fig. 12. FTIR spectra of pristine AP and AP containing residues.

their release engenders the formation of acid groups (O=)P–OH vibrating according to several frequency bands of weak intensity (wide peaks at 2820, 2300 and 1640 cm^{-1}). The hump between 1750 cm^{-1} and 1650 cm^{-1} ascribed to acids are confused with the peak at 1644 cm^{-1} attributed to aromatic C=C stretching vibrations.

IR spectra of alumina and aluminous residues are displayed Fig. 13. Several changes have to be noticed commonly with modified and unmodified alumina. First, nitrogenous compounds are not present anymore in the residue as showed by the disappearance of 1430–1420 cm^{-1} vibration. P=O band is shifted from 1215 to 1210 cm^{-1} with 15% AP to 1270 1260 cm^{-1} with oxides. Peak at 1047 cm^{-1} would be ascribed to P–O–P whereas P–O linked to aromatics would absorb around 965–960 cm^{-1} . Furthermore, aromatics compounds are clearly visible by the peak at 1610–1600 cm^{-1} , characteristic band of aromatics C=C. Contrary to

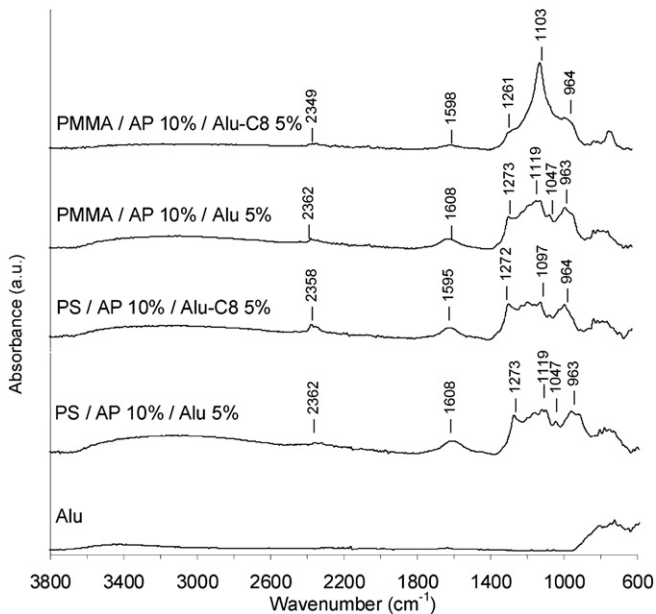


Fig. 13. FTIR spectra of alumina and alumina-containing residues.

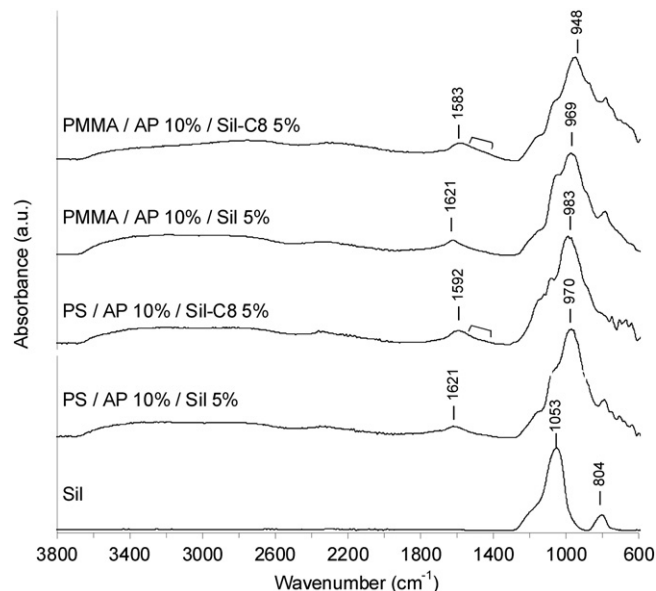


Fig. 14. FTIR spectra of silica and silica-containing residues.

free oxide residues, the hump at 1750–1650 cm^{-1} (P–OH) does not appear, which means that P–OH groups could react with aluminum oxides. Alkynes groups $\text{C}\equiv\text{C}$ resulting from dehydrogenation reactions absorb in IR at 2360–2350 cm^{-1} . The only difference between alumina based residues concerns the peak centred at around 1120–1100 cm^{-1} related to aluminum phosphate [27]. Indeed, an intense peak is observed at 1103 cm^{-1} of PMMA/AP 10%/Alu C8 5% residue corresponding to stretching vibration of PO_3^{2-} in crystalline phase AlPO_4 [28], which is in agreement with XRD pattern.

IR spectra of pyrogenic silica and siliceous residues are presented Fig. 14. Main absorption peaks of silica are centred at 1053 cm^{-1} ascribed to silica core and also at 782 cm^{-1} corresponding to deformation mode of Si–O (silanol groups). These bands appear in spectra of residues. Besides, aromatic compounds were exhibited by both P–O–Ar and C=C (aromatics) vibration mode, respectively at 980 970 cm^{-1} and 1620–1580 cm^{-1} . We have to notice that P=O vibration (at 1270 cm^{-1} for aluminous residues) does not appear which means that phosphoryl groups underwent reactions with other compounds. These reactions are likely to be in relation to silicon phosphate formation. Thus, “dissolution” of ammonium polyphosphate particles may occur in presence of silica which was confirmed by SEM in another study [29]. Finally, IR

Table 6
Assignment of the observed IR bands.

Bond	Vibration	cm^{-1}
O–H lié	Stretching	3500–3200
N–H	Stretching	3300–2600
C–C	Stretching	2380–2310
(O=)PO–H	Stretching	1740–1650
C=C Arom.	Stretching	1650–1550
NH_4^+	Deformation	1500–1340
P=O	Stretching	1315–1150
P–O	Sym. stretching	1080–1030
Si–O–Si	Stretching	1053
P–O–P	Sym. stretching	1030–955
P–O	Antisym. stretching	910–845
P–O–Ar	Stretching	995–900
Si–OH	Deformation	780
Al–O	Stretching	900–550

analyses show that modification of interphase promote char formation. Indeed, it is demonstrated not only by the shift of C=C aromatic vibration peak to 1590–1580 cm^{-1} but also by the band broadening towards lower wavenumbers (black mark on Sil C8 based spectra). This phenomenon results from the presence of polyaromatic species [30] liable to confer thermal stability for the char.

4. Conclusions

Synergies on fire properties in PMMA and PS have been investigated between nano sized oxides and ammonium polyphosphate flame retardant additives. The effect of modified nanoparticles was compared with the corresponding hydrophilic oxide nanoparticles as regards thermal and fire behaviour. Thermal degradation of mixed additives exhibited strong interactions between oxides and phosphorus flame retardant leading to modification of degradation pathway of AP. A second decomposition step no longer occurred in the presence of nanoparticles whereas hydrophobic silica delays first mass loss whose temperature range corresponds to octylsilane decomposition. Concerning thermal degradation of nano composites, only Sil C8 nanofiller delayed both PMMA and PS decomposition in the whole temperature range. Furthermore, synergy between AP and oxides was illustrated by the decrease of heat release rate compared to pure AP containing compositions. Two different kinds of char formation were observed according to the presence of alumina (shell structured char) or silica (bulk structured) with ammonium polyphosphate. Concerning surface modification, decrease of smoke opacity in cone calorimetry for PMMA/AP 10%/Alu C8 5% formulation could be linked not only to the catalytic effect of Alu C8 on thermal degradation of PMMA but also to the formation of AlPO_4 crystalline phase. Moreover, a noteworthy decrease of peak of heat release and smoke opacity as well as an increase of LOI were noticed with hydrophobic silica combined with AP both in PMMA and PS. This flame retardant behaviour was ascribed mainly to specific silicon metaphosphate (SiP_2O_7) crystalline phase which would contribute to promote charring and an efficient protection barrier.

Acknowledgements

We thank Clariant for donating phosphorus additives and Evonik for oxide nanoparticles.

References

- [1] Gilman J, Kashiwagi T, Lichtenham J. Nanocomposites: a revolutionary new flame retardant approach. *Sampe J* 1997;33:40–6.
- [2] Giannelis EP. Polymer-layered silicate nanocomposites. *Adv Mater* 1996;8:29–35.
- [3] Kashiwagi T, Grulke E, Hilding J, Harris R, Awad W, Douglas J. Thermal degradation and flammability properties of poly(propylene)/carbon nanotube composites. *Macromol Rapid Commun* 2002;23:761–5.
- [4] Laachachi A, Leroy E, Cochez M, Ferriol M, Lopez Cuesta JM. Use of oxide nanoparticles and organoclays to improve thermal stability and fire retardancy of poly(methyl methacrylate). *Polym Degrad Stab* 2005;89:344–52.
- [5] Zanetti M, Lomakin S, Camino G. Polymer layered silicate nanocomposites. *Macromol Mater Eng* 2000;279:1–9.
- [6] Jang BN, Costache M, Wilkie C. The relationship between thermal degradation behavior of polymer and the fire retardancy of polymer/clay nanocomposites. *Polymer* 2005;46:10678–87.
- [7] Lewin M. Reflections on migration of clay and structural changes in nanocomposites. *Polym Adv Technol* 2006;17:226–34.
- [8] Scharrel B, Bartolmai M, Knoll U. Some comments on the main fire retardancy mechanisms in polymer nanocomposites. *Polym Adv Technol* 2006;17:772–7.
- [9] Yang F, Nelson GL. Polymer/silica nanocomposites prepared via extrusion. *Polym Adv Technol* 2006;17:320–6.
- [10] Aruchamy A, Blackmore KA, Zelinski BJJ, Uhlmann DR, Booth C. *Mat Res Soc Symp P* 1992;249:353–7.
- [11] Hu YH, Chen CY, Wang CC. Viscoelastic properties and thermal degradation kinetics of silica/PMMA nanocomposites. *Polym Degrad Stab* 2004;84:545–53.
- [12] Laachachi A, Cochez M, Ferriol M, Lopez-Cuesta JM, Leroy E. Influence of TiO_2 and Fe_2O_3 fillers on the thermal properties of poly(methyl methacrylate) (PMMA). *Mater Lett* 2005;59:36–9.
- [13] Laachachi A, Ferriol M, Cochez M, Ruch D, Lopez-Cuesta JM. The catalytic role of oxide in the thermooxidative degradation of poly(methyl methacrylate) TiO_2 nanocomposites. *Polym Degrad Stab* 2008;93:1131–7.
- [14] Cinausero N, Azéma N, Lopez-Cuesta JM, Cochez M, Ferriol M. Impact of modified alumina oxides on the fire properties of PMMA and PS nanocomposites. *Polym Adv Technol*; 2010. doi:10.1002/pat.1695.
- [15] Laachachi A, Cochez M, Leroy E, Ferriol M, Lopez-Cuesta JM. Fire retardant systems in poly(methyl methacrylate): interactions between metal oxide nanoparticles and phosphinate. *Polym Degrad Stab* 2007;92:61–9.
- [16] Laachachi A, Cochez M, Leroy E, Gaudon P, Ferriol M, Lopez-Cuesta JM. Effect of Al_2O_3 and TiO_2 nanoparticles and APP on thermal stability and flame retardance of PMMA. *Polym Adv Technol* 2006;17:327–34.
- [17] Cui W, Guo F, Chen J. Preparation and properties of flame retardant high impact polystyrene. *Fire Saf J* 2007;42:232–9.
- [18] Camino G, Grassie N, McNeill IC. Influence of the fire retardant, ammonium polyphosphate, on the thermal degradation of poly(methyl methacrylate). *J Polym Sci* 1978;16:95–106.
- [19] Camino G, Luda MP. Mechanistic study on intumescence. In: Le Bras M, Camino G, Bourbigot S, Delobel R, editors. *Fire retardancy of polymers*, vol. 224. Royal Society of Chemistry; 1998. p. 48–63.
- [20] Castrovinci A, Camino G, Drevelle C, Duquesne S, Magniez C, Vouters M. Ammonium polyphosphate aluminum trihydroxide antagonism in fire retarded butadiene styrene block copolymer. *Eur Polym J* 2005;41:2023–33.
- [21] Czégény Z, Blazso M. Effect of phosphorus flame retardants on the thermal decomposition of vinyl polymers and copolymers. *J Anal Appl Pyroly* 2008;81:218–24.
- [22] Vippola M, Ahmaniemi S, Keranen J, Vuoristo P, Lepisto T, Mantyla T, et al. Aluminium phosphate sealed alumina coating: characterization of microstructure. *Mater Sci Eng* 2002;A323:1–8.
- [23] Hye-Jung H, Dong-Pyo K. Studies on curing chemistry of aluminium chromium phosphates as low temperature curable binders. *J Sol Gel Sci Techn* 2003;266:223–8.
- [24] Poojary DM, Borade RB, Campbell FL, Clearfield A. Crystal structure of silicon pyrophosphate (Form I) from powder diffraction data. *J Solid State Chem* 1994;112:106–12.
- [25] Riva A, Camino G, Fomperie L, Amigouët P. Fire retardant mechanism in intumescent ethylene vinyl acetate compositions. *Polym Degrad Stab* 2003;82:341–6.
- [26] Wang H, Wang Q, Huang Z, Shi W. Synthesis and thermal degradation behaviors of hyperbranched polyphosphate. *Polym Degrad Stab* 2007;92:1788–94.
- [27] Braun U, Scharrel B, Fichera MA, Jager C. Flame retardancy mechanisms of aluminum phosphinate in combination with melamine polyphosphate and zinc borate in glass-fibre reinforced polyamide 6,6. *Polym Degrad Stab* 2007;92:1528–45.
- [28] Mekky W, Nicholson PS. Nano-aluminum phosphate via a polymerized organic inorganic complex route. *J Mat Process Tech* 2007;190:393–6.
- [29] Cinausero N. Thermal degradation and fire reaction of PS and PMMA nanocomposites. PhD dissertation, Université de Montpellier; 2009. <http://tel.archives-ouvertes.fr/tel-00382965/fr/>.
- [30] Lin-Vien D, Colthup NB, Fateley WG, Grasselli JG. The handbook of infrared and Raman characteristic frequencies of organic molecules. San Diego: Academic Press; 1991.